



ELSEVIER

Available online at www.sciencedirect.com

SCIENCE @ DIRECT®

Journal of Non-Crystalline Solids xxx (2005) xxx–xxx

JOURNAL OF
NON-CRYSTALLINE SOLIDS

www.elsevier.com/locate/jnoncrysol

Crystallization behavior of a gas atomized Al₈₅Ni₁₀La₅ amorphous alloy

Zhihui Zhang^{a,*}, David Witkin^b, Enrique J. Lavernia^a

^a Department of Chemical Engineering and Materials Science, University of California, Davis, CA 95616, United States

^b Department of Chemical Engineering and Materials Science, University of California, Irvine, CA 92697, United States

Received 19 August 2004; received in revised form 5 April 2005

9 Abstract

10 Al₈₅Ni₁₀La₅ (at.%) alloy powders were fabricated using gas atomization. X-ray diffraction analysis revealed that powders in the
11 size range of <500 mesh (<25 μm) are amorphous. The crystallization behavior and kinetics of the amorphous Al₈₅Ni₁₀La₅ powders
12 (<25 μm) were investigated during continuous heating and isothermal annealing. The amorphous Al₈₅Ni₁₀La₅ alloy undergoes a
13 multi-step crystallization reaction in the temperature range of 250–390 °C. The activation energies for the first exothermic reactions
14 were determined as 344 kJ/mol. Instead of a primary crystallization, a eutectic reaction was found to be associated with the first
15 reactions and the crystalline phases were identified as fcc-Al, Al₁₁La₃, Al₃Ni and a metastable phase Al₃La. The isothermal anneal-
16 ing was carried out at temperatures of 235 °C, 245 °C and 250 °C. Results from the isothermal annealing analyses revealed presence
17 of quenched-in Al nuclei. The influence of isothermal annealing on the thermal stability of the Al₈₅Ni₁₀La₅ powders (<25 μm) is also
18 discussed.

19 © 2005 Published by Elsevier B.V.

20 *IDT*: A180; C290

21 *PACS*: 61.43.Dq; 61.46.+w; 64.70.Kb

23 1. Introduction

24 Interest in the study of high-strength and light-weight
25 materials has intensified in recent years, partly due to
26 rising energy costs. For aluminum alloys, an upper ten-
27 sile strength in the range of 550–600 MPa may be readily
28 achieved via age hardening, and usually does not exceed
29 700 MPa even when invoking other strengthening ap-
30 proaches, such as Hall–Petch strengthening, solid solu-
31 tion hardening, and dispersion strengthening [1]. The
32 theoretical shear strength for Al free of defects is esti-
33 mated as around 1500 MPa [2]. However, since the Al-
34 rich amorphous alloy family of Al–R–TM (R-rare earth

metal, TM-transition metal) was discovered [3,4], it has
been suggested that the tensile strength may reach as
much as 1500 MPa if this type of amorphous alloy is
partially devitrified and contains a microstructure con-
sisting of both nanocrystalline and amorphous phases
[5]. The dimensions of Al–R–TM amorphous alloys,
however, are currently limited to rapidly solidified pow-
ders or ribbons. Thus increasing efforts have been fo-
cused on producing bulk forms that retain a
nanocrystalline/amorphous microstructure after subse-
quent compaction and consolidation of the amorphous
precursors (gas-atomized powders and melt-spun rib-
bons, etc.) [5–7]. A clear understanding of their thermal
stability and the crystallization behavior is necessary to
control the compaction processes and achieve good
mechanical properties as well as microstructures, espe-

* Corresponding author. Tel.: +1 530 297 7251.

E-mail address: zhizhang@ucdavis.edu (Z. Zhang).

51 cially for controlling the precipitation of nanocrystalline
 52 aluminum crystallites, which are regarded as a likely
 53 source of the high strength for the alloys [2,5]. Precipita-
 54 tion of intermetallic compounds could further harden
 55 this alloy, but it is anticipated that they will diminish
 56 the ductility [8]. In the current study, the crystallization
 57 of an alloy with the atomic composition of $\text{Al}_{85}\text{Ni}_{10}\text{La}_5$
 58 is studied with particular attention to precipitation of
 59 the Al phase.

60 2. Experimental

61 The amorphous aluminum alloy powders used in the
 62 present investigation were prepared by gas atomization.
 63 A mixture of pure elemental Al (99.99 wt%), Ni
 64 (99.9 wt%) and La (99.9 wt%) with the nominal chemi-
 65 cal composition of $\text{Al}_{85}\text{Ni}_{10}\text{La}_5$ (at.%) was induction
 66 melted under a high-purity Ar atmosphere and then
 67 atomized at a superheat level of approximately 250 °C
 68 using high-purity He gas with an atomizing pressure of
 69 6.2 MPa. The powders were mechanically sieved at mesh
 70 sizes 500 (25 μm) and 270 (53 μm). X-ray diffraction
 71 analysis (XRD) showed that particles between 25 μm
 72 and 53 μm diameter were partially amorphous whereas
 73 particles less than 25 μm were essentially amorphous,
 74 as seen in Fig. 1(a). The amorphous nature of the
 75 $\text{Al}_{85}\text{Ni}_{10}\text{La}_5$ powders less than 25 μm was further con-
 76 firmed by transmission electron microscopy (TEM),
 77 shown in Fig. 1(b), although crystalline phases might
 78 be found in certain particles which, for whatever reason
 79 during the atomization process, had experienced a
 80 slower cooling history.

81 On the basis of these results, the atomized powders
 82 less than 25 μm were examined by means of differential
 83 scanning calorimetry (DSC) in terms of continuous heat-
 84 ing and isothermal annealing processes. DSC was carried
 85 out on a Perkin–Elmer DSC-7 using ultra-high purity N_2
 86 as the purging gas. The XRD analyses were carried out

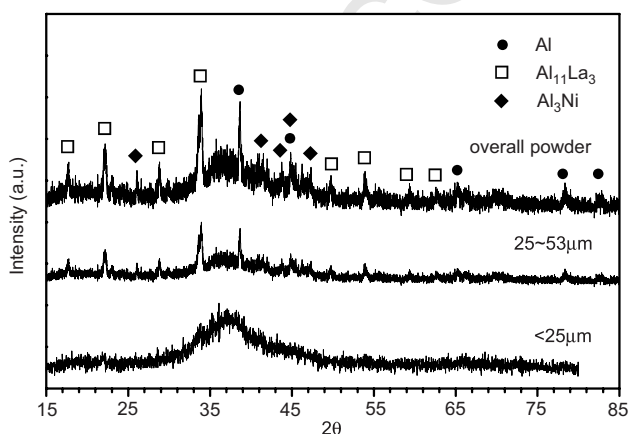


Fig. 1. XRD patterns of gas atomized $\text{Al}_{85}\text{Ni}_{10}\text{La}_5$ powders.

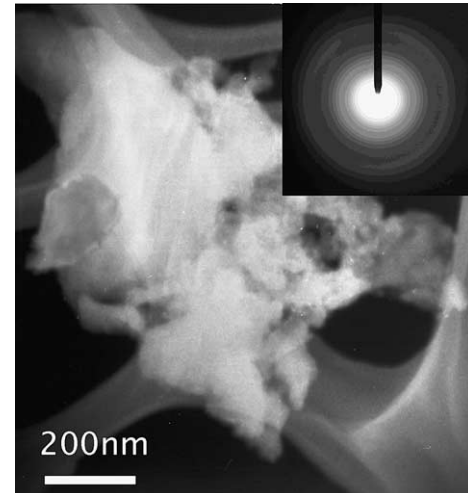


Fig. 2. TEM dark field micrograph and selected area diffraction pattern of amorphous $\text{Al}_{85}\text{Ni}_{10}\text{La}_5$ powders (<25 μm).

with a Scintag XDS 2000 X-ray diffractometer using
 CuK α radiation. TEM was carried out using a Philips
 CM-12 electron microscope operating at 100 kV. Addi-
 tional microscopic characterization of cross-sections of
 the devitrified powders was examined using a XL 30
 FEG scanning electron microscope (SEM) (Fig. 2).

3. Results

Fig. 3 shows the continuous heating DSC traces of
 the $\text{Al}_{85}\text{Ni}_{10}\text{La}_5$ amorphous powders (<25 μm) using
 heating rates from 2.5 °C/min to 40 °C/min. Crystalliza-
 tion processes occurred between 250 °C and 390 °C.
 Three distinct exothermic peaks were observed during
 the devitrification process. At high heating rates
 (>20 °C/min), a minor endothermic signal, indicating

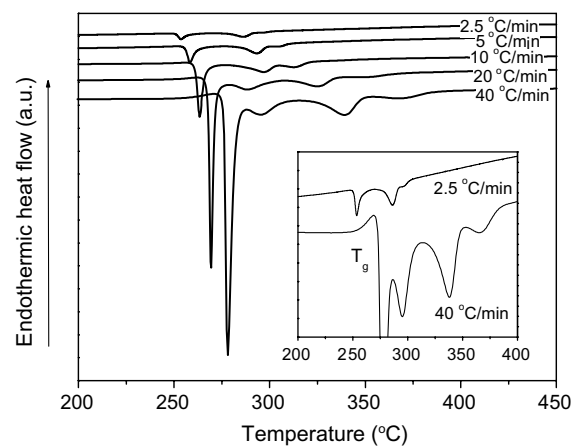
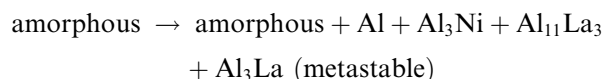


Fig. 3. Continuous heating DSC traces of $\text{Al}_{85}\text{Ni}_{10}\text{La}_5$ amorphous powders (<25 μm). The inset picture shows the enlarged curves for the heating rate of 40 °C/min and 2.5 °C/min.

101 the glass transition, was observed prior to the first crys-
 102 tallization peak, while another minor exothermic peak
 103 was found after the third exothermic peak. At low heat-
 104 ing rates ($<5\text{ }^\circ\text{C}/\text{min}$), the endothermic peak for glass
 105 transition was not resolved due to the fact that it over-
 106 lapped with the subsequent exothermic peak. In order
 107 to determine the crystallized phase corresponding to
 108 the first exothermic peak, the amorphous powders were
 109 heated to the peak temperature of $263\text{ }^\circ\text{C}$ at a heating
 110 rate of $10\text{ }^\circ\text{C}/\text{min}$ and held for 5 min. The heat-treated
 111 powders were then analyzed using XRD. The XRD re-
 112 sults showed the first exothermic peak corresponded to
 113 a eutectic-like reaction [9]:



115

116 The precipitated phases consisted of three equilibrium
 117 phases: Al, Al_3Ni , $\text{Al}_{11}\text{La}_3$ and a metastable phase
 118 Al_3La . XRD analysis of amorphous powders that were
 119 heated to $500\text{ }^\circ\text{C}$ indicated that the fully crystallized
 120 phases consisted only of Al, Al_3Ni and $\text{Al}_{11}\text{La}_3$; the
 121 metastable phase Al_3La had disappeared. In other
 122 words, the phase composition of the fully crystallized
 123 powder is the same as that of the coarse powders larger
 124 than $25\text{ }\mu\text{m}$.

125 In related studies [10–12], however, the first devitrifi-
 126 cation peak occurred in terms of the primary crystalliza-
 127 tion of fcc-Al and the activation energy for this reaction
 128 was found to be close to the self-diffusion activation
 129 energy of Al (144.2 kJ/mol). The apparent activation en-
 130 ergy controlling an exothermic reaction can be deter-
 131 mined by the Kissinger method [13].

$$133 \ln\left(\frac{v}{T_p^2}\right) = -\frac{E_a}{RT} + C,$$

134 where v is the heating rate, R is the gas constant, T is the
 135 characteristic temperature and can be frequently se-
 136 lected as the peak temperature T_p or the onset tempera-
 137 ture T_{on} . The term C is a constant ($C = Rk_0/E_a$, where k_0
 138 is the pre-exponential factor in the Arrhenius equation
 139 $k = k_0\exp(-E_a/RT)$). The respective activation energies
 140 are then determined from the slope of the curves
 141 $\ln(v/T_p^2)$ vs. $1/T_p$. The crystallization onset temperatures
 142 and the peak temperatures for the first three peaks deter-
 143 mined by DSC tracing are listed in Table 1. The plots of

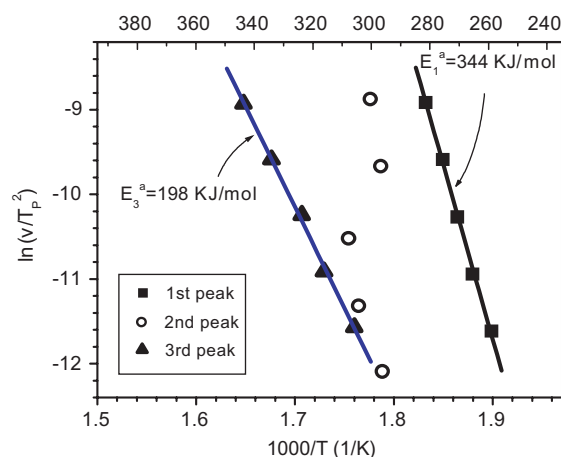


Fig. 4. Kissinger plots of gas atomized $\text{Al}_{85}\text{Ni}_{10}\text{La}_5$ powders.

144 $\ln(v/T_p^2)$ vs. $1/T_p$ are given in Fig. 4. The activation en-
 145 ergies corresponding the first peaks and the third peaks
 146 are linearly fitted to be 344 kJ/mol and 198 kJ/mol ,
 147 respectively. Again, the activation energy determination
 148 supported the conclusion that the first peak underwent a
 149 reaction other than the precipitation of fcc-Al. The sec-
 150 ond peaks do not exhibit a linear relationship and it is
 151 probably because the reactions are sensitive to tempera-
 152 tures and thus the activation energies are temperature
 153 dependent.

154 Precipitation of nanosized fcc-Al phase is favored be-
 155 cause the amorphous $\text{Al}_{85}\text{Ni}_{10}\text{La}_5$ alloy will be further
 156 hardened due to dispersions of nanoscale Al crystallites
 157 [5] as well as the solute concentration enrichment in the
 158 amorphous matrix [14]. Precipitation of intermetallic
 159 compounds could further increase the hardness but is
 160 anticipated to decrease the ductility of this alloy [8].
 161 As a result, it is necessary to examine the conditions that
 162 might promote the precipitation of fcc-Al and retard the
 163 occurrence of intermetallic compounds. To investigate
 164 these possible conditions, the amorphous $\text{Al}_{85}\text{Ni}_{10}\text{La}_5$
 165 alloy powders were subjected to isothermal annealing
 166 below the glass transition temperature.

167 Isothermal DSC traces of the $\text{Al}_{85}\text{Ni}_{10}\text{La}_5$ amor-
 168 phous powders are shown in Fig. 5. The samples were
 169 heated to temperatures of $235\text{ }^\circ\text{C}$, $245\text{ }^\circ\text{C}$ and $250\text{ }^\circ\text{C}$,
 170 respectively, at a heating rate of $200\text{ }^\circ\text{C}/\text{min}$ and held

Table 1
Onset and peak temperatures of the exothermic reactions at various heating rates

Heating rate ($^\circ\text{C}/\text{min}$)	First peak		Second peak		Third peak	
	Onset ($^\circ\text{C}$)	Peak ($^\circ\text{C}$)	Onset ($^\circ\text{C}$)	Peak ($^\circ\text{C}$)	Onset ($^\circ\text{C}$)	Peak ($^\circ\text{C}$)
2.5	249.8	253.6	269.3	286.2	–	295.2
5	253.1	259.0	276.6	293.8	298.3	305.3
10	258.8	263.4	276.7	297.0	304.7	312.9
20	264.6	267.6	276.8	286.6	306.4	323.6
40	268.5	272.8	282.9	290.0	310.9	333.8

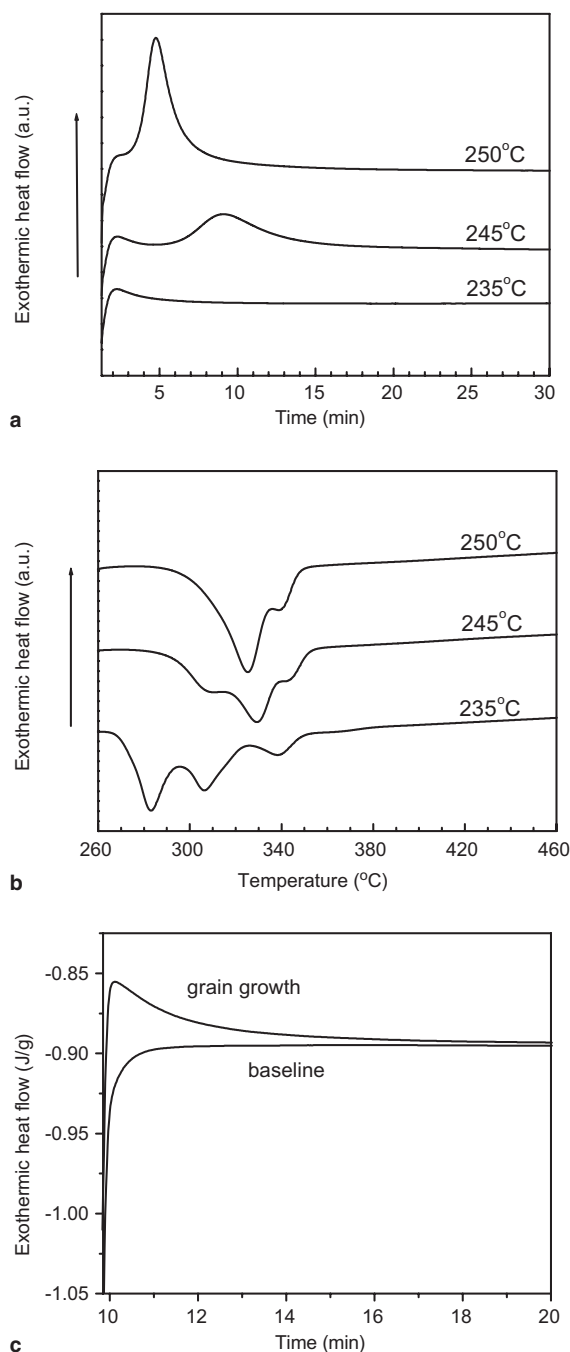


Fig. 5. Isothermal annealing of $\text{Al}_{85}\text{Ni}_{10}\text{La}_5$ amorphous powders (<25 μm) at 235 °C, 245 °C and 250 °C (a). Continuous heating traces of the powders annealed at 235 °C, 245 °C and 250 °C (b). Isothermal tracing at 235 °C showing a monotonically decreasing signal (c).

171 for 30 min (Fig. 5(a)), followed by continuous heating to
 172 500 °C at a rate of 40 °C/min (Fig. 5(b)). The holding
 173 temperature 250 °C was selected on the basis of the on-
 174 set temperature of the first crystallization peak at a slow
 175 heating rate (2.5 °C/min). Exothermic bell-shaped peaks
 176 occurred in the isothermal curves at 245 °C and 250 °C
 177 and the exothermic peaks overlapped in the subsequent

continuous DSC tracing from the holding temperature 178
 to 500 °C. However, a monotonically decreasing signal 179
 was observed in the isothermal DSC curve of 235 °C 180
 and the three distinct exothermic peaks were clearly re- 181
 solved in the subsequent continuous temperature scan. 182
 In order to rule out that the signal may have been the 183
 result of an instrumental artifact due to heat flow over- 184
 shoot, a quality-assurance test was completed using a 185
 heating rate of 20 °C/min, followed by re-running the 186
 temperature program with the transformed sample after 187
 it had cooled to room temperature, as shown in Fig. 188
 5(c). The baseline signal gave a perfect horizontal line 189
 indicating that the monotonically decreasing signal re- 190
 sulted from phase transformation in the sample. There- 191
 fore the $\text{Al}_{85}\text{Ni}_{10}\text{La}_5$ amorphous alloy showed different 192
 crystallization behavior during holding at 235 °C from 193
 above 245 °C. 194

The transformation process during the isothermal 195
 ageing was further analyzed using the Johnson–Mehl– 196
 Avrami (JMA) phenomenological model [15]: 197

$$\zeta = 1 - \exp(-k(t - \tau)^n), \quad 199$$

where ζ is the transformed volume fraction, n is the Av- 200
 rami exponent which depends on the transformation 201
 mechanism, and τ is the incubation time at which a re- 202
 gion nucleates. The term k is the reaction constant. 203

An isothermal calorimetry signal showing a mono- 204
 tonically decreasing curve is evidence of growth from 205
 pre-existing nuclei, and leads to an Avrami exponent n 206
 that is less than 1. In contrast, the presence of a peak 207
 suggests a nucleation and growth process where the Av- 208
 rami exponent n turns out to be greater than 1 [16]. The 209
 specific value of n can be obtained by fitting the curves 210
 of transformed volume fractions vs. the annealing time. 211
 As shown in Fig. 6(a) and (b), when the $\text{Al}_{85}\text{Ni}_{10}\text{La}_5$ 212
 amorphous alloy was annealed at 235 °C, the data from 213
 Fig. 5(c) was fitted to the JMA equation, giving an Av- 214
 rami exponent equal to 0.87. For annealing at 245 °C 215
 and 250 °C, the transformed volume fractions calculated 216
 from Fig. 5(a) are shown in Fig. 6(a) and the Avrami 217
 plots of $\ln(-\ln(1 - \zeta))$ vs. $\ln(t)$ are given in Fig. 6(b). 218
 The Avrami exponents at 245 °C are equal to 3.3 at the 219
 initial stage and then decrease to 1.9 at the final 220
 stage. In the case of 250 °C, the Avrami exponent starts 221
 at 3.9 before finally decreasing to 1.7. The non-linear 222
 nature of the Avrami plots implies that the transforma- 223
 tion mechanisms have changed in the final crystalliza- 224
 tion stage. The XRD patterns for the samples 225
 annealed at 235 °C, 245 °C and 250 °C are shown in 226
 Fig. 7. It is observed that only precipitation of the fcc- 227
 Al phase occurred at 235 °C. At 245 °C, the Al phase 228
 and intermetallic compounds $\text{Al}_{11}\text{La}_3$, Al_3Ni and Al_3La 229
 formed in a eutectic-like reaction. The phases formed 230
 during annealing at 250 °C were apparently similar to 231
 those observed at 245 °C. For comparison, the XRD 232
 pattern for the powders that were annealed at 283 °C 233

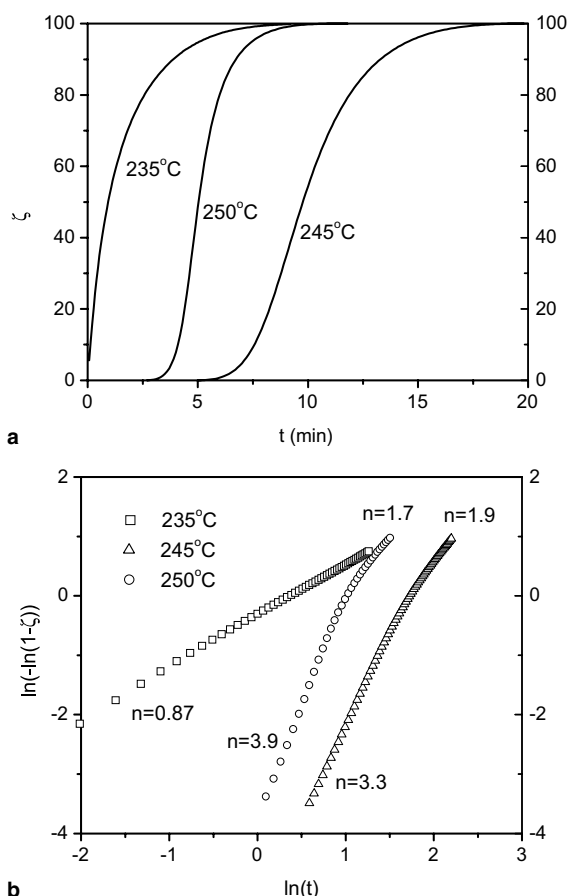


Fig. 6. Plots of transformed volume fraction vs. annealing time (a) and the Avrami plots (b).

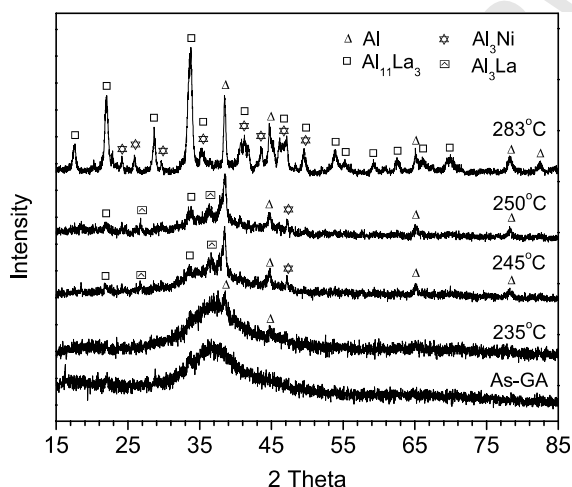


Fig. 7. XRD patterns of $\text{Al}_{85}\text{Ni}_{10}\text{La}_5$ powders (<25 μm) annealed at various temperatures compared to the as-atomized (GA) powders.

234 for 5 min is also plotted in Fig. 7. It can be seen that the
 235 metastable phase Al_3La has disappeared under the
 236 annealing condition.

4. Discussion

237

238 The present results show that amorphous $\text{Al}_{85}\text{Ni}_{10}\text{La}_5$ 238
 239 powders can be produced by gas atomization, at least 239
 240 under the experimental conditions used herein. The 240
 241 intermetallic phases do not precipitate, even as the 241
 242 matrix is heated up to an annealing temperature of 242
 243 235 °C. The observation of a monotonically decreasing 243
 244 signal during the isothermal DSC tracing performed at 244
 245 235 °C suggests a growth reaction [16,17], indicating 245
 246 the presence of quenched-in nuclei in the amorphous 246
 247 matrix. As seen in Fig. 7, only fcc-Al phase was detected 247
 248 after annealing at 235 °C. In contrast, observation of an 248
 249 exothermic peak suggested a nucleation and growth 249
 250 reaction during isothermal annealing at 245 °C and 250
 251 250 °C. This divergence in devitrification behavior was 251
 252 in agreement with the subsequent continuous DSC scans 252
 253 following the isothermal annealing. As shown in Fig. 253
 254 5(b), the three exothermic reactions, which can be seen 254
 255 in the continuous heating curves (Fig. 3), are well-de- 255
 256 fined in the powders annealed at 235 °C but could not 256
 257 be resolved any more in the powders annealed at 257
 258 245 °C and 250 °C. It suggests that the exothermic peaks 258
 259 in Fig. 5(a) are those missing first peaks in Fig. 5(b). The 259
 260 reaction products also support this suggestion. The crys- 260
 261 talline phases (i.e., Al, $\text{Al}_{11}\text{La}_3$, Al_3Ni and Al_3La) 261
 262 formed at 245 °C and 250 °C are the same as those 262
 263 formed at the peak temperature 263 °C.

264 At a temperature of 245 °C, the Avrami exponent is 264
 265 3.3 at the initial stage, followed by a decrease to 265
 266 1.9. At 250 °C, the Avrami exponent is 3.9 at the initial 266
 267 stage and decreases to 1.7 in the late stage. The value of 267
 268 Avrami exponents between 3 and 4 has been interpreted 268
 269 as interface-controlled growth of nuclei with decreasing 269
 270 nucleation rate, while Avrami exponents in the range of 270
 271 1.5 to 2.5 correspond to diffusion-controlled growth 271
 272 with a decreasing nucleation rate [15]. In the early 272
 273 stages, if assumptions of spatially randomly distributed 273
 274 nuclei are made, two typical cases can be considered: 274
 275 an Avrami exponent of 3 implies zero nucleation rates 275
 276 and the Avrami exponent of 4.0 means constant nuclea- 276
 277 tion rates [18]. It is implied that the nucleation sites 277
 278 are nearly saturated at 245 °C while nucleation rates 278
 279 are close to constant at 250 °C. As shown in Fig. 5(a), 279
 280 a longer incubation period was observed at 245 °C than 280
 281 at 250 °C. The presence of an apparent incubation peri- 281
 282 od at 245 °C and 250 °C also indicated that the nuclei 282
 283 were newly created during the incubation period and 283
 284 different from the quenched-in nuclei observed at 284
 285 235 °C. The assumption of random nucleation is sup- 285
 286 ported by electron microscopic observation. Fig. 8(a) 286
 287 shows an SEM micrograph for the cross-section of the 287
 288 partially crystallized powders after annealing at 250 °C 288
 289 for 0.5 h. The back-scattered electron image exhibits a 289
 290 featureless surface, indicating the size of the crystalline 290
 291 particles is beyond the instrumental resolution and no 291

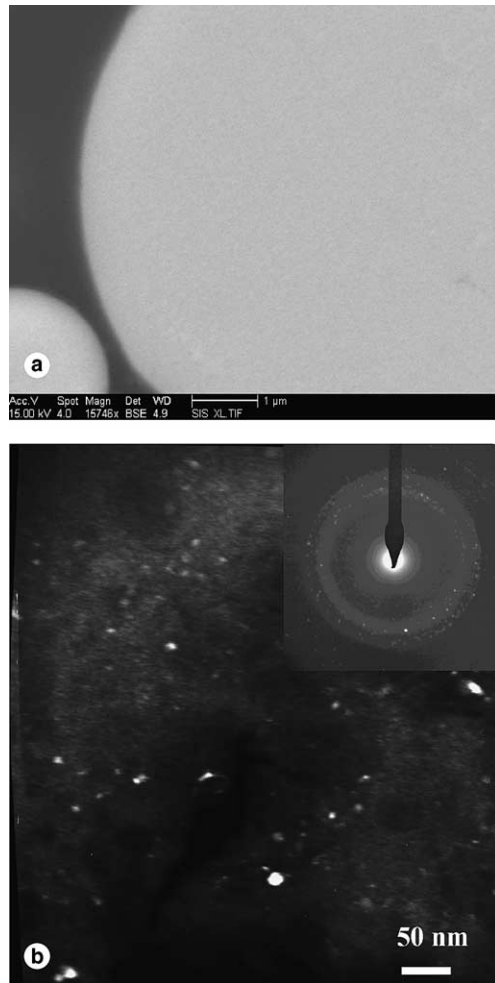


Fig. 8. Microstructures for the $\text{Al}_{85}\text{Ni}_{10}\text{La}_5$ powders ($<25\ \mu\text{m}$) held at $250\ ^\circ\text{C}$. (a) SEM back-scattered electron image for the powder cross-section. (b) TEM dark field image and selected area diffraction pattern (inset).

292 particles larger than 100 nm are observed. Fig. 8(b)
 293 shows the TEM dark field image for powders subjected
 294 to the same thermal treatment. It can be seen that the
 295 size of the nanocrystallites is around 10–30 nm and they
 296 are randomly distributed in the amorphous matrix. Dur-
 297 ing the later stages, the observed drop in the values of
 298 the Avrami exponent is perhaps attributed to the fact
 299 that growth of Al crystallite becomes dominant. As
 300 shown in Fig. 8(b), the SADP mainly comes from con-
 301 tribution of the Al crystallites. As the eutectic reaction
 302 occurs, precipitation of compounds will lead to deple-
 303 tion of La and Ni in the local areas. This will destabilize
 304 the amorphous matrix and induce diffusion of Al. As a
 305 result, diffusion-controlled growth of Al crystallites be-
 306 comes more significant during the later stages.

307 For Al-based amorphous alloys, a primary crystalli-
 308 zation of fcc-Al has often been suggested as the first
 309 transformation reaction [5,10–12,19]. In the case of
 310 Al–Ni–La alloys, the primary formation of fcc-Al was

311 also observed in an $\text{Al}_{89}\text{La}_6\text{Ni}_5$ alloy [10] and an Al_{88} -
 312 La_6Ni_6 alloy [12]. However, a eutectic reaction instead
 313 of a primary reaction corresponding to the first peak
 314 was recently identified in the same chemical composition
 315 of $\text{Al}_{89}\text{La}_6\text{Ni}_5$ [9]. In the current study, the first peaks in
 316 continuous DSC tracing correspond to a eutectic-like
 317 reaction associated with precipitation of the stable phase
 318 fcc-Al, Al_3Ni , $\text{Al}_{11}\text{La}_3$ and a metastable phase Al_3La .
 319 The XRD traces do not allow a simple identification
 320 of the phases precipitated during the second and the
 321 third peaks. By comparing the change of XRD peak
 322 intensities due to the second reactions, it implies that
 323 precipitation of the compounds also presents in the
 324 second reactions. The second peaks failed to fit the Kis-
 325 singer equation and their positions changed abnormally
 326 with increasing heating rate. From Table 1 it can be seen
 327 that the onset temperatures for the second peaks were in
 328 the range of $269\ ^\circ\text{C}$ to $283\ ^\circ\text{C}$. The Al_3La phase was not
 329 observed in the powders held at $283\ ^\circ\text{C}$ for 5 min. Hence
 330 the second peak may be mainly related to formation of
 331 the La-rich phases. Studies of Al–Ni–Y and Al–Ni–Ce
 332 alloys suggested that the rare earth metals had lower
 333 mobility than Al as well as Ni [14]. Hence it is reason-
 334 able to assume that La also has lower mobility. It should
 335 be pointed out that the eutectic-like reaction requires
 336 long-range diffusion of La, the reaction however might
 337 not be simply diffusion-controlled and the rate-control-
 338 ling mechanisms are sensitive to the temperatures.
 339 Hence the activation energy failed to attain a constant
 340 value, which could be attributed to a variation of the
 341 rate controlling mechanisms due to increasing tempera-
 342 ture. Meanwhile a decrease of lanthanum concentration
 343 will destabilize the amorphous matrix and allow forma-
 344 tion of the Al_3Ni phase.

345 It has been suggested that partially crystallizing an
 346 amorphous alloy with nanosized Al crystallites dis-
 347 persed in the amorphous matrix would further enhance
 348 its mechanical properties and the Al phase would be ob-
 349 tained on basis of a primary crystallization reaction
 350 [2,5,8,20]. In the gas atomized $\text{Al}_{85}\text{Ni}_{10}\text{La}_5$ amorphous
 351 powders, quenched-in Al nuclei were found and the
 352 nanosized Al crystal could be developed by annealing
 353 the amorphous powders below the glass transition tem-
 354 perature. The size of the Al crystallite held at $235\ ^\circ\text{C}$ for
 355 0.5 h was around 5–20 nm based on TEM observations.
 356 It is noteworthy that precipitation of the elemental Al
 357 phase implies that the remnant amorphous phase be-
 358 comes enriched with solute elements, especially near
 359 the aluminum crystals. These increased concentrations
 360 will stabilize the amorphous phase and impede crystalli-
 361 zation [14,21]. Comparing Figs. 3 and 5(b), it can be
 362 seen that the first peak temperature shifted from
 363 $273\ ^\circ\text{C}$ to $277\ ^\circ\text{C}$ after the amorphous powder was held
 364 at $235\ ^\circ\text{C}$ for 0.5 h. When we increased the ageing time
 365 from 0.5 h to 1 h, the peak shifted from $277\ ^\circ\text{C}$ to
 366 $283\ ^\circ\text{C}$ using the same heating rate of $40\ ^\circ\text{C}/\text{min}$, as

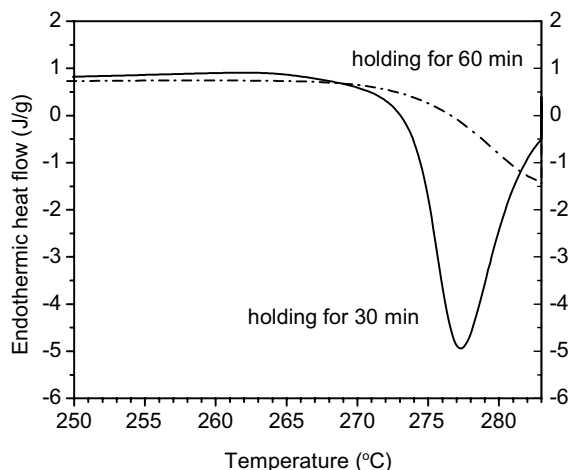


Fig. 9. Continuous DSC traces showing that the thermal stability can be improved by a pre-annealing at 235 °C.

367 shown in Fig. 9. This suggests that while nanoscale Al
368 crystallites are being formed through growth the ther-
369 mal stability of the amorphous phase has been
370 increased.

371 5. Conclusions

372

373 (1) $\text{Al}_{85}\text{Ni}_{10}\text{La}_5$ powders were produced using gas
374 atomization. The powder fraction with a particle
375 size less than 25 μm was amorphous. The amor-
376 phous phase is stable during heating up to a tem-
377 perature of 235 °C. An annealing treatment at
378 this temperature could improve the thermal stabil-
379 ity of the amorphous phase.

380 (2) Isothermal DSC traces indicate that quenched-in
381 Al nuclei existed in the amorphous matrix.
382 Transformation at 235 °C exhibited growth of alu-
383 minium nuclei. Crystallization above 245 °C exhib-
384 ited a nucleation and growth process associated
385 with a eutectic-like reaction. The eutectic-like reac-
386 tion instead of a primary crystallization took place
387 in the first exothermic peaks, during which fcc-Al

phase was precipitated concurrently with interme- 388
tallic compounds of $\text{Al}_{11}\text{La}_3$ and Al_3Ni as well as a 389
metastable phase Al_3La . 390

391

Acknowledgments

392

The authors would like to acknowledge the Army Re- 393
search Office (Grant No. DAAD 19-03-1-0020 and 394
Grant No. DAAD19-01-1-0627) for financial support. 395
Particular thanks also go to Dr William Mullins for 396
his support and assistance. 397

References

398

- [1] J.-P. Immarigeon, R.T. Holt, A.K. Koul, L. Zhao, W. Wallace, J.C. Beddoes, *Mater. Charact.* 35 (1995) 41. 399
400
[2] H.S. Kim, P.J. Warren, B. Cantor, H.R. Lee, *Nanostruct. Mater.* 11 (1999) 241. 401
402
[3] Y.H. Kim, A. Inoue, T. Masumoto, *Mater. Trans. JIM* 31 (1990) 747. 403
404
[4] Y. He, S.J. Poon, G.J. Shiflet, *Science* 241 (1988) 1640. 405
[5] A. Inoue, *Prog. Mater. Sci.* 43 (1998) 365. 406
[6] S.J. Hong, T.S. Kim, H.S. Kim, W.T. Kim, B.S. Chun, *Mater. Sci. Eng. A* 271 (1999) 469. 407
408
[7] O.N. Senkov, D.B. Miracle, J.M. Scott, S.V. Senkova, *J. Alloys Compd.* 365 (2004) 126. 409
410
[8] T.S. Kim, S.J. Hong, B.T. Lee, *Mater. Sci. Eng. A* 363 (2003) 81. 411
[9] Y.X. Zhuang, J.Z. Jiang, Z.G. Lin, M. Mezouar, W. Crichton, A. Inoue, *Appl. Phys. Lett.* 79 (2001) 743. 412
413
[10] F. Ye, K. Lu, *J. Non-Cryst. Solids* 262 (2000) 228. 414
[11] O.N. Senkov, J.M. Scott, D.B. Miracle, *J. Alloys Compd.* 337 (2002) 83. 415
416
[12] P. Si, X. Bian, W. Li, J. Zhang, Z. Yang, *Phys. Lett. A* 319 (2003) 424. 417
418
[13] H.E. Kissinger, *Anal. Chem.* 29 (1957) 1702. 419
[14] X.Y. Jiang, Z.C. Zhong, A.L. Greer, *Mater. Sci. Eng. A* 226–228 (1997) 789. 420
421
[15] J.W. Christian, *The Theory of Transformations in Metals and Alloys*, Pergamon, Oxford, 2002, pp. 529–546. 422
423
[16] L.C. Chen, F. Spaepen, *J. Appl. Phys.* 69 (1991) 679. 424
[17] L.C. Chen, F. Spaepen, *Nature* 336 (1988) 366. 425
[18] A.L. Greer, *Acta Metall.* 30 (1982) 171. 426
[19] J.H. Perepezko, R.J. Hebert, R.I. Wu, G. Wilde, *J. Non-Cryst. Solids* 317 (2003) 52. 427
428
[20] T. Gloriant, A.L. Greer, *Nanostruct. Mater.* 10 (1998) 389. 429
[21] D.R. Allen, J.C. Foley, J.H. Perepezko, *Acta Mater.* 46 (1998) 430
431
432